



Effect of calcination temperature on magnetic, structural, thermal and optical properties of BFO-T nanoparticles

Harminder Singh¹ · Jaspreet Kaur Rajput²

Received: 16 March 2020 / Accepted: 25 June 2020 / Published online: 3 July 2020
© Springer Nature Switzerland AG 2020

Abstract

BFO-T (BiFeO_3) nanoparticles have been prepared via auto-combustion technique using tartaric acid as a chelating agent. Role of chelating agent and effect of different calcination temperatures on the structural, morphological, optical, thermal and magnetic behaviour were demonstrated. The properties related to phase structure, surface morphology, thermal stability were investigated by XRD, TEM and TGA respectively. Fourier Transformed Infrared spectra of BFO-T nanoparticles calcinated at different temperatures showed various types of bond formations in the samples. The average particle size of BFO-T nanoparticles were found to be in the range 6–30 nm at different calcinated temperature. The optical band gaps of pure BFO-T nanoparticles were estimated using the Tauc's equation which was found to be 2.20 eV. Magnetic measurement of pure BFO-T nanoparticles indicated ferromagnetic behavior with saturation magnetization of 0.36 emu/g.

Keywords BFO-T nanoparticles · Magnetic · Auto combustion · Band gap · Calcination

1 Introduction

Multiferroic materials are a class of materials that got immense interest owing to the coexistence of electrical and magnetic properties. In addition, multiferroic materials have potential applications in field of spin valves, information storage devices, microelectronic devices spintronic devices, and sensors [1]. Among various multiferroic materials, magneto electric multiferroic are one of the most commonly studied materials in which magnetization can be affected by electric field and vice-versa. A number of single phase magneto electric multiferroic materials have been reported so far, however, most of them are insufficient because of chemical and physical incompatibility between ferroelectric and ferromagnetic ordering [2, 3]. In view of this, Multiferroic BiFeO_3 (BFO) nanoparticles are found to be newly emerging material with practical applications in various fields of electrical, magnetic and optical devices [4, 5]. Multiferroic BFO are concurrently

subsistence of both the ferroelectric and antiferromagnetic properties at room temperature with tunable structure, Curie (≈ 1100 K) and Neel (≈ 643 K) temperature [6]. Multiferroic BFO possesses a perovskite type unit cell, having rhombohedral phase with point group $R3c$. Its unit cell have a lattice parameter, a_{rh} , of 3.965\AA and a rhombohedral angle, α_{rh} , of ca. $89.3\text{--}89.48^\circ$ at room temperature [7]. Multiferroic BFO are also known for its intriguing optical properties such as light-induced size changes, anomalous photovoltaic effect, persistent photoconductivity and switchable diode effects [8]. At the nanoscale BFO exhibit tremendous novel physical properties that are different from the bulk counter parts which make them potential candidates for the use in future electronic nano devices [9]. Further, due to its narrow band gap (2.1–2.7 eV) and high chemical stability, it has enormous appliances as photo catalyst for the waste water treatment [10, 11]. A number of reports in the literature have been found for its use as

✉ Harminder Singh, Harmindersingh87@gmail.com | ¹Department of Chemistry, DAV University, Jalandhar, Punjab 144001, India. ²Department of Chemistry, Dr. B R Ambedkar National Institute of Technology, Jalandhar, Punjab 144011, India.



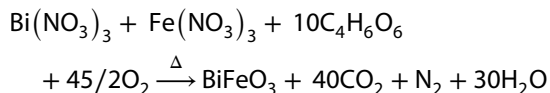
magnetically recoverable visible light photocatalyst for the degradation of industrial effluents [12–15].

Due to wide spread applications of Multiferroic BFO, number of techniques are used for the preparation of BFO nanoparticles, however, each of them has their own advantages and limitations [10]. Thus, development of Multiferroic BFO nanoparticles with high purity, uniform size, and homogeneous morphology is still in demand. In light of this, here, we are using an auto-combustion technique for the synthesis new BiFeO₃-tartaric acid (BFO-T) nanoparticles by using tartaric acid as a chelating agent. We have used the auto combustion technique for the preparation of BFO-T nanoparticles as it is the one of the most promising techniques for the synthesis of numerous high purity nanomaterials. In addition, this technique is found to be straightforward, proficient, cost effective, and swift in nature. To our pleasure, we were successful in preparation of highly pure form of BFO-T nanoparticles where the sample had undergone calcination at different range of temperature such as 150 °C, 450 °C, 550 °C, 650 °C and 750 °C. Further, the extensive study of effect of different range of calcination temperature on purity, surface area, surface morphology, optical, thermal stability, crystalline and local structure of as-synthesized nanoparticles were studied. To the best of our knowledge there is no report in literature where the properties of BFO-T nanoparticles calcinated at different temperature have been discussed. The prepared pure BFO-T nanoparticles exhibited ferromagnetic behaviour, which can be used as magnetic recoverable catalyst in organic synthetic transformations. optical properties showed that these materials can be used as visible light photo catalyst for the degradation of industrial effluents and can be used for potential applications in optoelectronic devices.

2 Experimental

For the synthesis of BFO-T nanoparticles, Bi(NO₃)₃·5H₂O, Fe(NO₃)₃·9H₂O and tartaric acid were taken as 1:1:2 mmol, respectively. Metal precursors, Bi(NO₃)₃·5H₂O and Fe(NO₃)₃·9H₂O (as in 1:1 mmol) were dissolved in distilled water and 3 M HNO₃ (as in 1:2 ml), respectively, followed by sonication for 10 min. After this, the two solutions were mixed and undergone sonication for 15 min more. Then chelating agent tartaric acid (2 mmol) was added to the reaction mixture. For homogeneous mixing, the mixture was stirred for 30 min at 800 rpm. The mixture was then heated on hot plate at 100 °C for 30 min. The black powder obtained was then undergone calcination at 150 °C, 450 °C, 550 °C, 650 °C and 750 °C temperature for one hour.

During the calcination process, the complexing agent decomposes and the mass of gases generated (like CO₂, N₂ etc.) leads to the creation of highly crystalline and single phased perovskite BFO-T nanoparticles as shown below:



3 Characterization

The crystal structure of prepared magnetic nanoparticles catalyst was investigated by X-ray diffraction (XRD) using a Panalytical XPERTPRO (NPD) X-ray diffractometer with Cu K α radiation ($\lambda = 0.154$ nm), in the 2θ range 10°–80°. Fourier transform IR (FT-IR) spectroscopy was carried out by using Agilent Cary 600 in the range 400–4000 cm^{−1}. The morphology was studied using transmission electron microscopy (TEM). The sample was prepared by dispersion of nanoparticles in ethanol, which were deposited on a carbon-coated Cu grid, and after drying, analysis was performed using a Hitachi S7500 instrument. The magnetic properties were measured using a vibrating sample magnetometer (VSM, Princeton Applied Research model155) at room temperature with a maximum magnetic field range of + 1 T to − 1 T. Thermogravimetric analysis (TGA) was performed on the catalyst using an EXSTAR6000TG/DTA 6300 instrument in the temperature range 50–700 °C at a heating rate of 10 °C/min under nitrogen atmosphere. Surface area and pore characteristics were characterized using Quanta Chrome Nova-1000 surface analyzer instrument under liquid nitrogen temperature with vacuum degassing at 110 °C for 3 h. The specific surface area was calculated using the BET equation. Raman spectra were recorded on Renishaw Invia Raman Microscope equipped with argon laser (514 nm) as source of excitation.

4 Result and Discussion

4.1 3.1 Structural and morphology analysis

The Fourier Transformed Infrared (FT-IR) spectra of BFO-T nanoparticles were recorded at different calcinated temperatures as shown in Fig. 1.

In a case of BFO-T nanoparticles calcinated at 150 °C, a wide peak in the range from 3000–3400 cm^{−1} was observed which was ascribed to the OH stretching mode of the water molecules. However, with increase in the calcination temperature from 150 °C to 650 °C, it was found

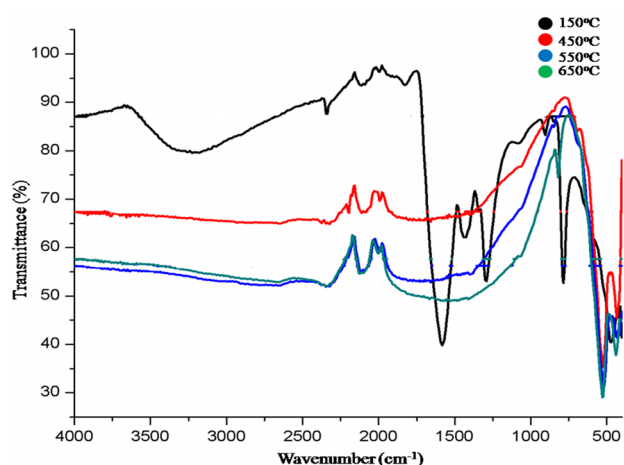


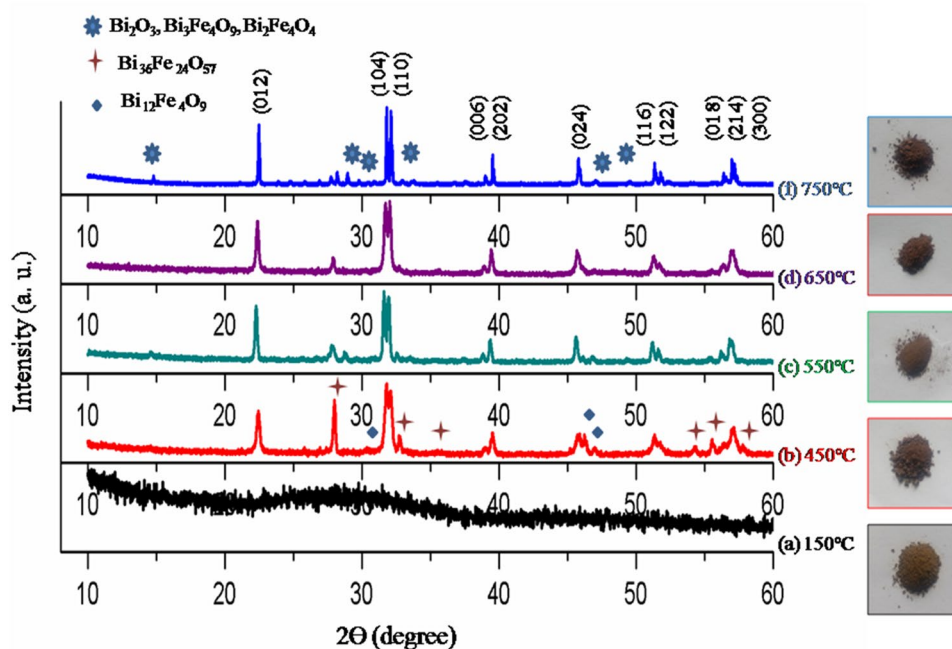
Fig. 1 Comparison study of Fourier transform infrared (FT-IR) spectra of BFO-T nanoparticles calcinated at 150 °C, 450 °C, 550 °C, and 650 °C

that, the intensity of this peak goes on decreasing from the surface of samples, indicating the removal of the water molecules from the sample. Further, BFO-T nanoparticles with calcination temperatures 150 °C, 450 °C and 550 °C showed the presence of peaks in the range from 1628–1672 cm^{-1} of symmetric bending vibration of C=O, 1375–1440 cm^{-1} of symmetric bending vibration of C–H bond and 1275–1282 cm^{-1} of stretching vibration of C–O of tartaric acid precursor [16]. The existence of these peaks was due to the fact that during auto combustion, a huge amount of energy was released in the form of gases forming a partially crystalline form of product, consisting of

organic chelating agents and metal residual precursors, respectively. From this observation, we found that more thermal treatment is required to obtain pure crystalline form of the BFO-T nanoparticles. So when sample was further calcinated at higher temperature i.e. 650 °C, no such kinds of peaks have been observed or we can say that there was no tartaric acid remained in the sample [17]. In addition, BFO-T nanoparticles at 650 °C showed strong peaks at 433 cm^{-1} , 517 cm^{-1} and 819 cm^{-1} , which were ascribed to the stretching and bending vibrations of Bi–O and Fe–O bonds [16]. Moreover, during calcination at higher temperature (650 °C), impurities were released as CO_2 and H_2O from the reaction mixture.

To characterize the stable single phase of materials, XRD spectra of BFO-T nanoparticles was recorded when calcinated at a different range of temperatures i.e. 150 °C, 450 °C, 550 °C, 650 °C and 750 °C as shown in Fig. 2. The XRD spectrum of BFO-T nanoparticles at low temperature i.e. 150 °C showed no characteristic peak, indicating the amorphous nature of the material. However, the main diffraction peaks of BFO-T nanoparticles started appearing at 450 °C along with secondary minor impurity phases like $\text{Bi}_2\text{Fe}_4\text{O}_9$ and $\text{Bi}_{36}\text{Fe}_{24}\text{O}_{57}$ corresponding to $2\theta = 30.35^\circ$, 47.01° , 48.32° and 27.81° , 32.80° , 35.60° , 48.51° , 55.28° , 56.23° and 57.77° , respectively. The appearance of secondary impurity phases was due to the comparable oxygen affinity of both Fe and Bi ions. On further increasing temperature around 550 °C, the intensity of secondary phases decreases along with the sharpening of major diffraction peaks of BFO-T nanoparticles.

Fig. 2 XRD analysis of BFO-T nanoparticles calcinated at (a) 150 °C, (b) 450 °C, (c) 550 °C, (d) 650 °C, (e) 750 °C



When the sample was further calcinated at 650 °C, the main diffraction peaks of BFO-T nanoparticles were observed at 22.33°, 31.57°, 32.04°, 38.87°, 39.37°, 45.66°, 51.33°, 51.69°, 56.25°, 56.81° and 57.12° corresponding to (012), (104), (110), (006), (202), (024), (116), (122), (214), (018) and (300) Miller indices, respectively. All the major peaks accurately harmonized with the JCPDS Card no. 86–1518 [6]. The above results indicating that sample BFO-T nanoparticles prepared at 650 °C have more sharpened diffraction peaks along with the exact exclusion of secondary phases. It can also be observed that the majority of the peaks of BFO-T nanoparticles belong to distorted rhombohedral structure of BiFeO₃ nanoparticles. From the above studies it was concluded that upon increasing calcination temperature, pure form of the BFO-T nanoparticles was obtained [18, 19], *i.e.* pure perovskite form of BFO-T nanoparticles was obtained [1]. This result was also in concord as discussed earlier in FT-IR analysis. We also compared the diffraction peaks of BFO-T nanoparticles calcinated at 750 °C with the sample calcinated at 650 °C. We found that new impurity peaks was observed at $2\theta = 14.67^\circ, 28.83^\circ, 29.61^\circ, 33.62^\circ, 47.03^\circ$ and 49.30° , which may be attributed to the formation of Bi₂O₃, Bi₃Fe₄O₉ [1] and Bi₂Fe₄O₄ [20]. Thus, indicated that 650 °C was the optimum calcination temperature for the formation of

single phase perovskite form of BFO-T nanoparticles. At this temperature, all the secondary phases were removed entirely and pure form of single phase BFO-T nanoparticles was generated. Further, the average particle size of BFO-T nanoparticles were calculated using Scherrer's formula, $D = k\lambda/\beta \cos \Theta$, where λ is the wavelength, β is the corrected diffraction line full-width at half maximum, k is a constant (having a value of 0.94) and Θ is Bragg's angle [21], by using different planes like (012), (104) and (110). The calculated average size for BFO-T nanoparticles calcinated at different temperatures 150 °C, 450 °C, 550 °C, 650 °C and 750 °C was found to be 6.0 nm, 13.26 nm, 14.35 nm, 30.0 nm and 45.2 nm, respectively as shown in Table 1. The increase in average particles size with increasing calcination temperature was ascribed due to the formation of cluster and owing to the particle collision [22]. Further, the enhancement in diffraction peaks intensity and diffraction peak sharpness with an increase in temperature was responsible for increase in particle size of BFO-T nanoparticles at higher temperature [23]. In addition to that as there were different types of impurity phases were formed as discussed above, their amount of formation be calculated by XRD and have been illustrated in Table 2.

To further investigate the particle size and morphology of the prepared BFO-T nanoparticles, transmission electron microscopy (TEM) was performed using carbon coated copper grid as shown in Fig. 3.

The grain size obtained by TEM analysis (20 nm and 42 nm for calcination temperature of 150 °C and 650 °C respectively) was little bit large as compared to the average size calculated by XRD analysis (6.0 nm and 30 nm for calcination temperature 150 °C and 650 °C respectively). This was due to the fact that grain contains sub-grains, which were separated by low-angle grain boundaries [24]. Furthermore, no agglomeration of particles was observed as the particles were well dispersed before the TEM analysis [23], thus large size was observed in TEM studies.

Table 1 Average particle size calculated by XRD of BFO-T nanoparticles prepared at different temperature

Sr.no	Sample (BiFeO ₃)(BFO-T)	Average particle size (nm)
1	BFO-T-150 °C	6.0
2	BFO-T-450 °C	13.26
3	BFO-T-550 °C	14.35
4	BFO-T-650 °C	30.0
5	BFO-T-750 °C	45.2

Table 2 Amount of different phases calculated from XRD of BFO-T nanoparticles prepared at different temperature

Calcination temp/ impurity phases	★ Bi ₃₆ Fe ₂₄ O ₅₇ (%)	◆ Bi ₁₂ Fe ₄ O ₉ (%)	✱ Bi ₂ O ₃ , Bi ₃ Fe ₄ O ₉ and Bi ₂ Fe ₄ O ₄ (%)
150 °C	At this temperature, BFO-T showed no characteristic peak, indicating the amorphous nature of the material		
450 °C	80, 34.51, 16.13, 20.54, 29.13 at $2\theta = 27.77^\circ$, 34.51°, 35.40°, 53.97° and 55.50° respectively	34.67, 36.25, 19.04, at $2\theta = 45.71^\circ, 45.86^\circ$ and 30.32° respectively	–
550 °C	32.17, 22.03, 15.30, 18.72, 22.00 at $2\theta = 27.77^\circ$, 34.51°, 35.40°, 53.97° and 55.50° respectively	17.13, 18.96, 18.01, at $2\theta = 45.71^\circ, 45.86^\circ$ and 30.32° respectively	–
650 °C	0.01 at $2\theta = 27.77^\circ$	–	–
750 °C	–	–	15.95, 19.75, 20.79, 9.74, 8.17 at $2\theta = 14.67^\circ, 28.83^\circ, 29.61^\circ, 33.62^\circ, 47.03^\circ$ and 49.30° respectively

Fig. 3 TEM image of BFO-T nanoparticles calcinated at **a** 150 °C and **b** 650 °C

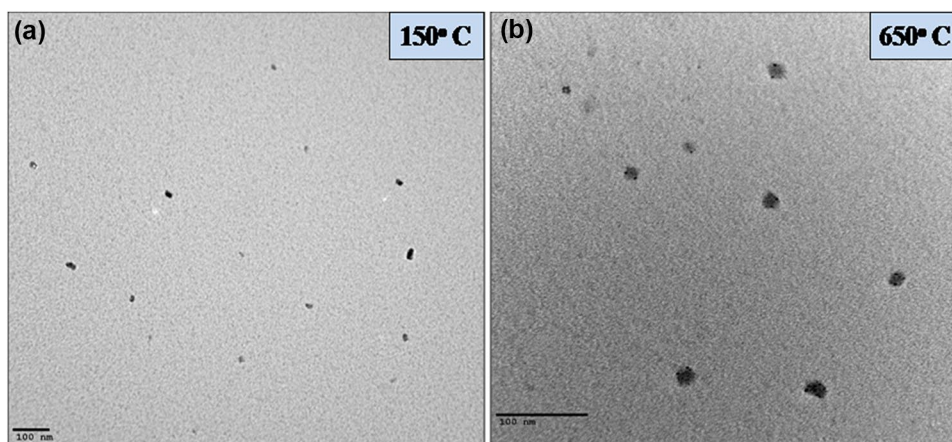


Table 3 Surface area and pore volume analysis of samples of BFO-T nanoparticles prepared at different temperature

Sr.no	Sample (BiFeO ₃)(BFO-T)	Surface area (m ² /g)
1	BFO-T-150 °C	16.828
2	BFO-T-450 °C	15.040
3	BFO-T-550 °C	9.201
4	BFO-T-650 °C	4.595

The investigation of surface area was carried out by using BET studies. The results obtained from BET analysis of BFO-T nanoparticles calcinated at the different range of temperature has been shown in Table 3 and Fig. 4.

As expected, the surface areas of BFO-T nanoparticles were reduced with increase in calcination temperature. This was due to the increase in particle size with increase in calcination temperature as calculated by XRD analysis. Thus, the result obtained for BFO-T nanoparticles from BET analysis were consistent with the XRD analysis. It was observed that calcinated at higher temperature leads to decrease in the number of nitrates molecules which resulted in increment in the size of BFO-T nanoparticles. Moreover, at highest temperature 650 °C, the BFO-T nanoparticles are in the most crystalline form, thus, have the smallest surface area [25].

5 Analysis of optical properties

In order to examine the optical properties, UV–vis analysis of synthesized BFO-T nanoparticles calcination at different temperature i.e. 150 °C, 450 °C, 550 °C and 650 °C was carried out as shown in Fig. 5. The Tauc's equation was used for the estimation of the band gap, $(\alpha h\nu)^n = B(h\nu - E_g)$, where α , h , ν , E_g , and B are the absorption coefficient, Plank constant, light frequency, band gap energy and a

constant respectively. For BiFeO₃, $n = 2$, which indicates the direct band gap. The band gap energy was calculated by extrapolating the linear portion of $(\alpha h\nu)^2$ vs $h\nu$ to the point $\alpha = 0$ [14].

The value of the band gap for the samples prepared at 150 °C, 450 °C, 550 °C, and 650 °C was 2.56 eV, 2.40 eV, 2.26 eV and 2.20 eV, respectively Fig. 6. It has been observed that the value of band gap decreases with increase in calcinated temperature. This was due to the increase in average particle size of BFO-T nanoparticles at high temperature, which resulted in "quantum size effect". This "quantum size effect" leads to decrease in the E_g values with increase in particle size of the nanoparticles [26, 27]. In addition, the obtained least band gap i.e. 2.20 eV for BFO-T nanoparticles calcinated at 650 °C temperature was in agreement with the previous literature values [13, 14]. This value also demonstrated that the prepared BFO-T nanoparticles are suitable for performing as a photocatalyst for the degradation of harmful compounds in the range of visible light.

6 Analysis of magnetic properties

Further, we also studied the magnetic behavior of the prepared BFO-T nanoparticles by VSM technique. For this, the study of magnetic hysteresis $M(H)$ of samples calcinated at the different range of temperatures was carried out at room temperature over a magnetic field of ± 1 T as shown in Fig. 7. All the prepared samples of BFO-T nanoparticles showed narrow hysteresis cycle which indicated their soft magnetic character. It is also well known that the magnetic character possessed by the BFO nanoparticles were due to the existence of Fe³⁺ and excess of O vacancies [1]. The values of saturation magnetization (M_s) for BFO-T nanoparticles synthesized at different calcination temperature are 0.32 emu/g, 5.72 emu/g, 5.56 emu/g and 0.36 emu/g for 150 °C,

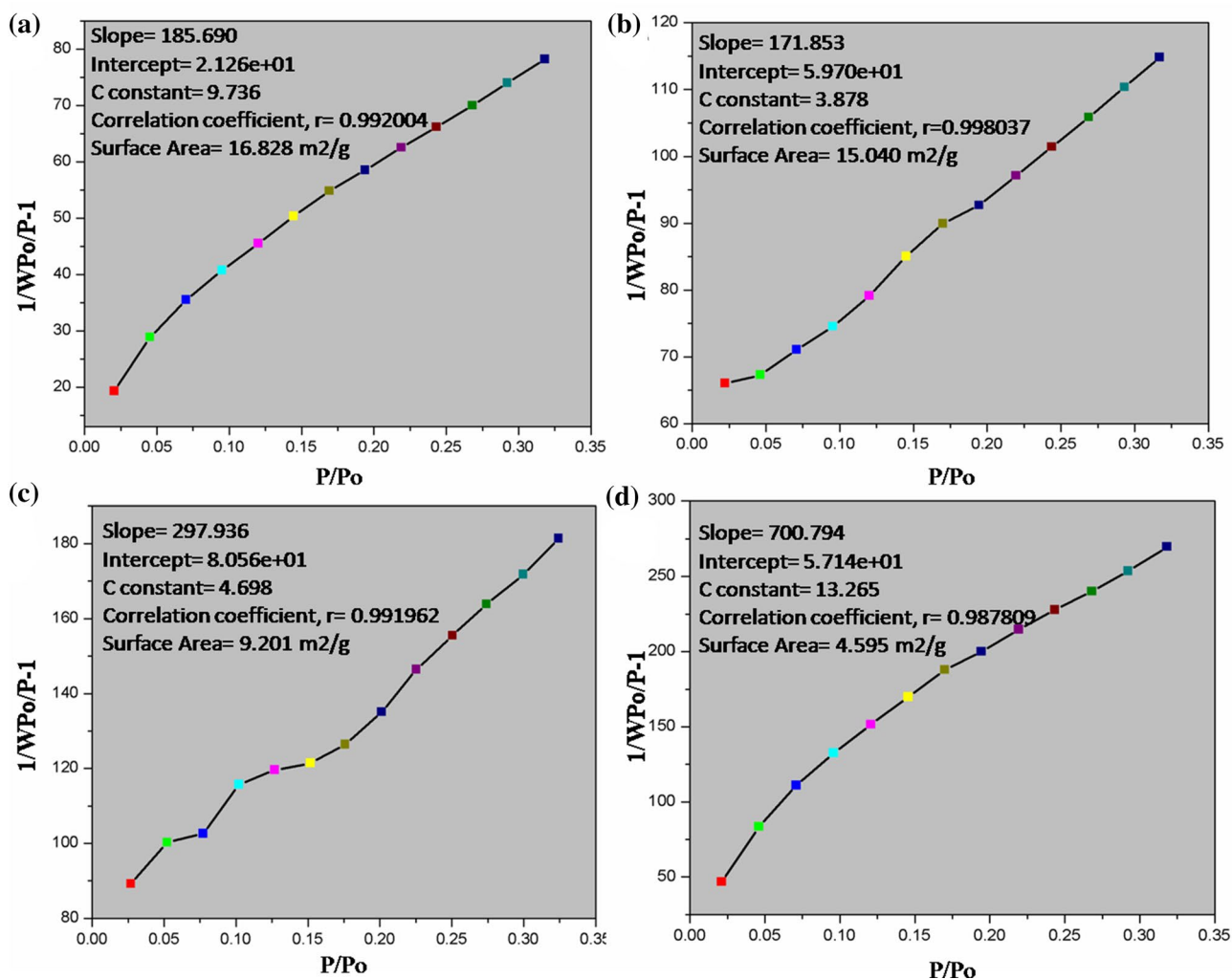


Fig. 4 Surface area analysis of BFO-T nanoparticles calcinated at **a** 150 °C, **b** 450 °C, **c** 550 °C, **d** 650 °C

450 °C, 550 °C and 650 °C, respectively. The low saturation magnetization value of the sample calcinated at 150 °C was might be due to the little bit formation of Fe–O, O–Fe–O bonds as also revealed by the FT-IR analysis. Further, increase in the M_s value was observed at high calcinated temperature *i.e.* at 450 °C and 550 °C. This abrupt increase in the M_s value was due to complete formation of Fe–O and O–Fe–O bonds in the prepared BFO-T nanoparticles. However, at 650 °C, again decrease in the magnetization value was observed which was due to the increase in the bond length of Bi–Fe bond and bond angle of Fe–O–Fe, O–Fe–O bonds [28].

Another reason for a decrease in the value of magnetic saturation with increasing calcination temperature was due to the fact that some grains at higher temperature do not possess a spontaneous magnetic moment

and therefore they were not capable to contribute in the magnetization [16]. The value of M_s *i.e.* 0.36 emu/g clearly confirmed the ferromagnetic character of pure form of BFO-T nanoparticles obtained at 650 °C [29]. Further, the observed value of magnetization saturation was enough to separate the BFO-T nanoparticles from the reaction mixture by applying strong magnet, which further enhanced its use as a magnetically separable catalyst in the organic reactions [30].

7 Analysis of thermal properties

For the determination of chemical stability of as synthesized nanoparticles, thermal gravimetric analysis (TGA) of BFO-T nanoparticles prepared by calcination at 150 °C and 650 °C was carried out as shown in Fig. 8.

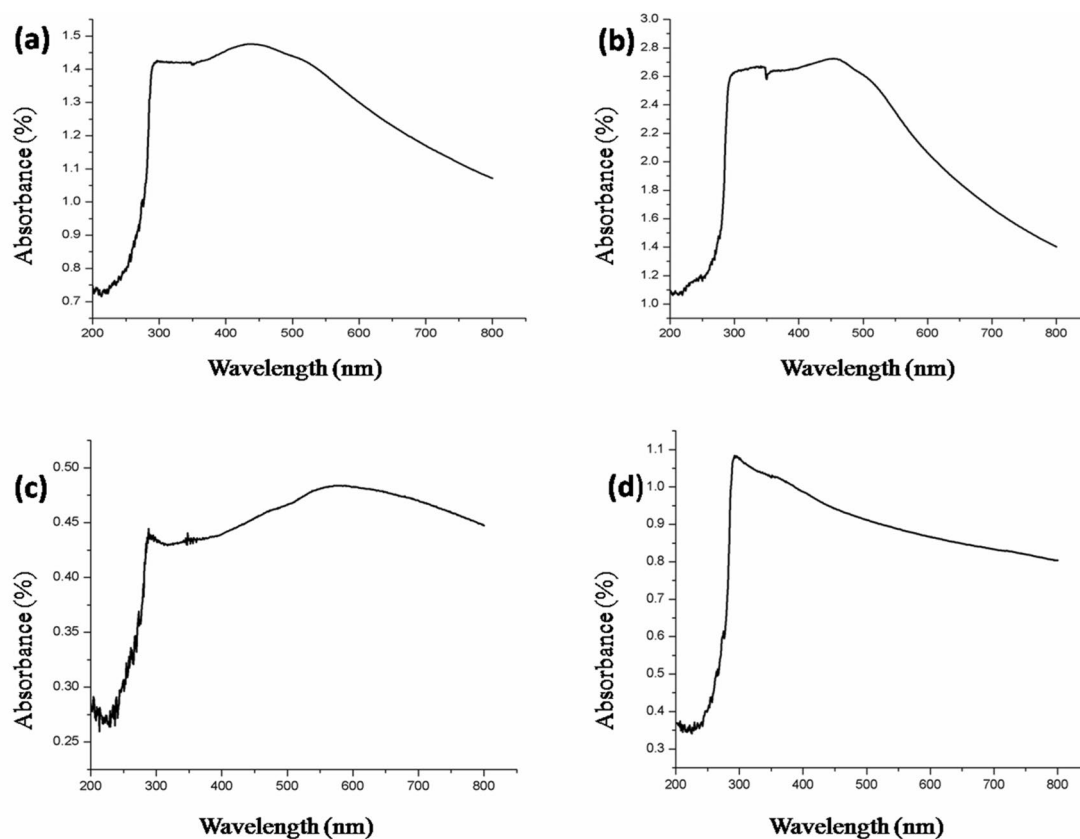


Fig. 5 UV-Vis spectra of BFO-T nanoparticles calcinated at **a** 150 °C, **b** 450 °C, **c** 550 °C, and **d** 650 °C

It has been found that the initial weight loss of 0.12% from 0–264 °C ascribed to the loss of surface hydroxyl group from the surface of nanoparticles. This loss was also well matched with the FT-IR analysis demonstrated earlier. On further increasing the temperature from 264–402 °C, weight loss observed was 0.15%, which verified that reaction starts occurring at this temperature range and leads to the formation of BFO-T nanoparticles. A small weight loss (0.09%) was also observed in the range of 402–584 °C, which may be attributed to the decomposition of organic impurities before 584 °C [23]. Further decrease in weight loss (above 584 °C) was due to the decomposition of nitrate species. It was also observed that, with increasing calcination temperature the stability of BFO-T nanoparticles increases, as weight percentage left for the samples calcinated at 150 °C and 650 °C was 87.79 and 99.66, respectively. The reason for higher weight percentage left with increasing temperature from 150 °C to 650 °C could be ascribed to the formation of stable single phase of BFO-T nanoparticles which was demonstrated by XRD results earlier.

8 Analysis of crystalline and local structure

For the investigation of crystalline and local structure of as synthesized nanoparticles Raman spectroscopy was used. Raman spectrum of BFO-T nanoparticles calcinated at 650 °C (as it was observed as the final optimized calcination temperature for the formation of BFO-T nanoparticles as proved by XRD results) was recorded as shown in Fig. 9.

According to the symmetry consideration, the 13 Raman active modes ($4A_1 + 9E$) for BFO having distorted rhombohedral structure with $R3c$ space group should be observed [31]. In our case, three intense peaks at 131 cm^{-1} , 167 cm^{-1} , 210 cm^{-1} and a weak intensity peak at 474 cm^{-1} were observed which were assigned for $4A_1$ modes. The peaks around 112 cm^{-1} , 115 cm^{-1} , 259 cm^{-1} , 272 cm^{-1} , 351 cm^{-1} , 361 cm^{-1} , 457 cm^{-1} , 471 cm^{-1} and 538 cm^{-1} were assigned for the $9E$ modes. The appearance of modes above 200 cm^{-1} was due to the internal vibrations of FeO_6 octahedra and modes below 200 cm^{-1} were caused by the Bi atoms of the perovskite layer which corresponds to a rigid layer [32]. The above results were in good agreement with the XRD studies and previous reports, thus, confirming the perovskite structure of BFO-T nanoparticles [33].

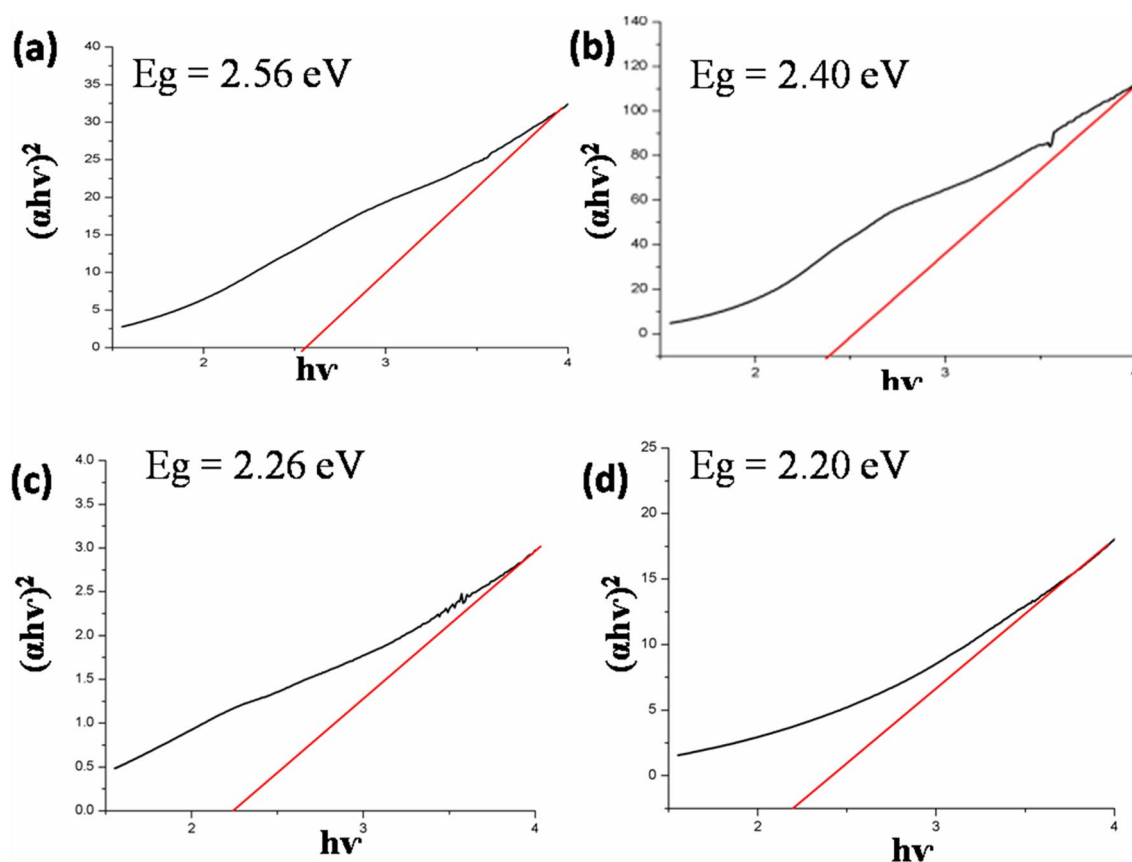


Fig. 6 Band gap values of BFO-T nanoparticles calcinated at **a** 150 °C, **b** 450 °C, **c** 550 °C, and **d** 650 °C

9 Conclusion

In conclusion, we have synthesized the single phase highly pure BFO-T nanoparticles by auto-combustion route via tartaric acid as a chelating agent. The adopted methodology is simple, cost effective, and efficient. FT-IR studies confirmed the presence of Bi-O and Fe-O bonds in the prepared BFO-T nanoparticles. Effect of different calcination temperature (150°, 450 °C, 550 °C, 650 °C and 750 °C) on various properties of prepared BFO-T nanoparticles had been explored. XRD analysis of prepared BFO-T nanoparticles confirmed that calcination temperature 650 °C is the optimum calcination temperature to obtain the highly pure BFO-T nanoparticles. The particle size of as synthesized nanoparticles was studied by XRD and TEM techniques followed the same trend that particle size increased with increase in calcination temperature. Raman

spectroscopy also confirmed the perovskite structure of the prepared pure BFO-T nanoparticles. VSM study confirmed its ferromagnetic character, which can be used as magnetic recoverable catalyst in organic synthetic transformations. In optical band gap study, the value of band was decreased with increase in calcination temperature; this observation was owing to “quantum size effect”. This effect leads to decrease in the E_g values with increase in particle size of the nanoparticles as in our case particle size increased with increase in calcination temperature. Further, this studied showed that these can be used as visible light photo catalyst for the degradation of industrial effluents. In addition, pure phase BFO-T nanoparticles having ferromagnetic and optical properties in visible region may also be used for potential applications in optoelectronic devices.

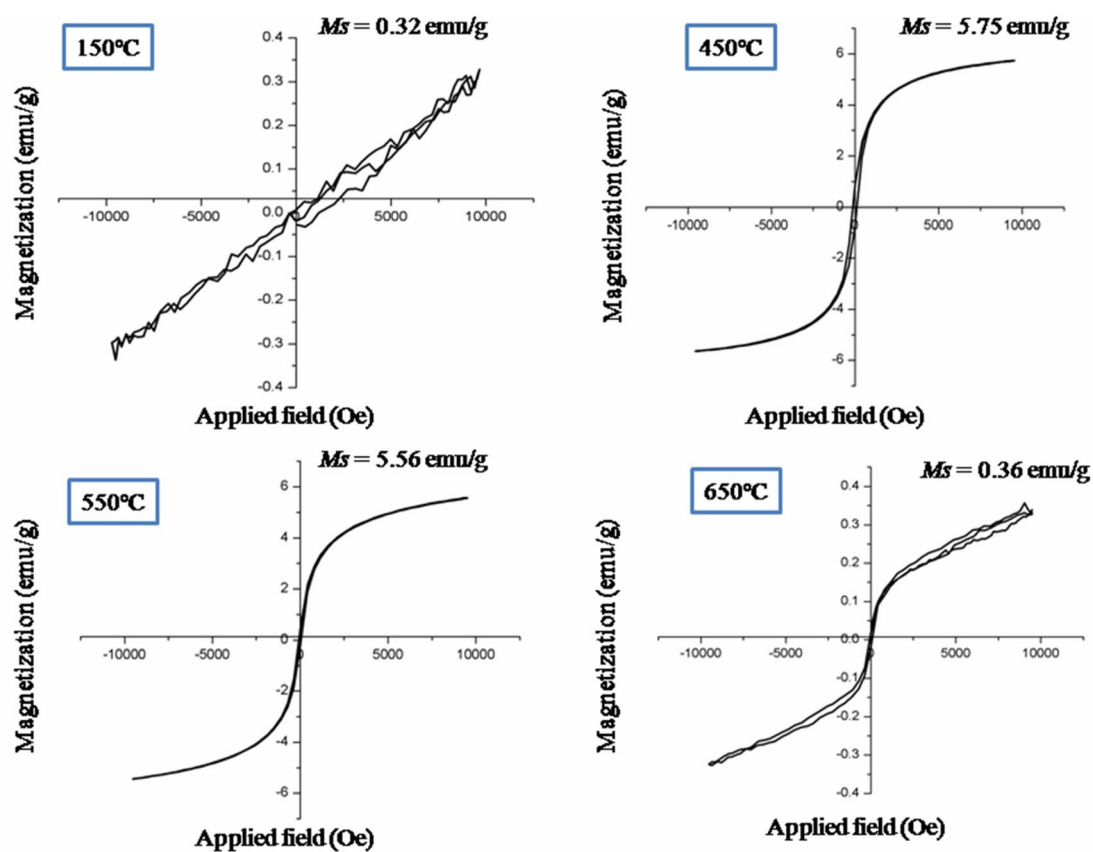


Fig. 7 VSM of BFO-T nanoparticles calcinated at 150 °C, 450 °C, 550 °C and 650 °C

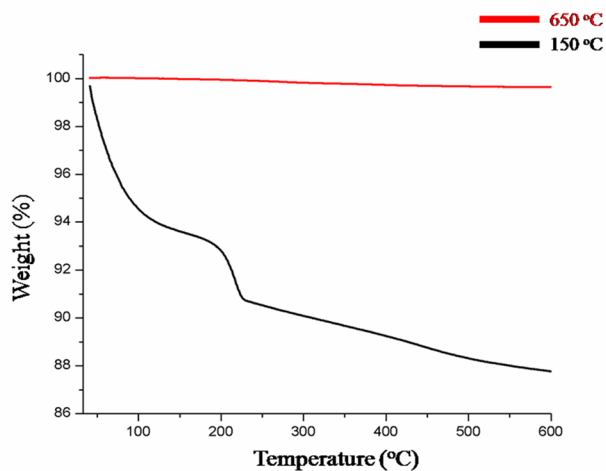


Fig. 8 TGA analysis of BFO-T nanoparticles calcinated at 150 °C, and 650 °C

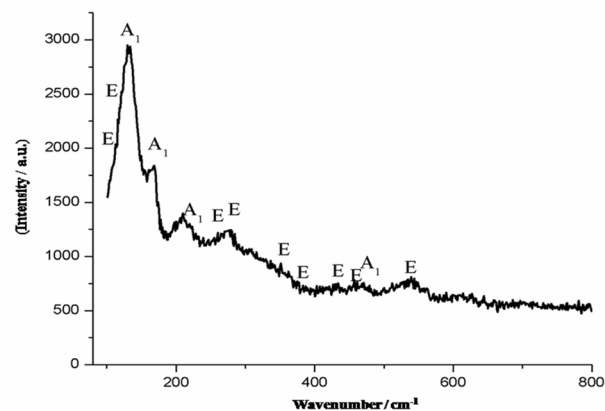


Fig. 9 Raman Spectra of BFO-T nanoparticles synthesized by Tartaric acid as chelating agent and calcinated at 650 °C

Acknowledgements We are thankful to CIL, IIT Roorkee for VSM, BIT Bengaluru for BET, SAIF, Panjab University Chandigarh for TEM and XRD, NIT Hamirpur for Raman spectroscopy and Department of Chemistry NIT Jalandhar for FT-IR and TGA.

Compliance with ethical standards

Conflict of interest The authors have no conflict of interest.

References

- Manzoor A, Afzal AM, Umair M, Ali A, Rizwan M, Yaqoob MZ (2015) Synthesis and characterization of Bismuth ferrite (BiFeO_3) nanoparticles by solution evaporation method. *J Magn Magn Mater* 393:269–272. <https://doi.org/10.1016/j.jmmm.2015.05.066>
- Narayan S, Mishra BG, Shirolkar MM, Sen S, Das SR, Janes DB (2013) Structural, microstructural and magneto-electric properties of single-phase BiFeO_3 nanoceramics prepared by auto-combustion method. *Mater Chem Phys* 141:423–431. <https://doi.org/10.1016/j.matchemphys.2013.05.040>
- Taylor P, Wang KF (2009) Multiferroicity: the coupling between magnetic and polarization orders. *Adv Phys* 58:321–448. <https://doi.org/10.1080/00018730902920554>
- Fiebig M, Lottermoser T, Fröhlich D, Goltsev AV, Pisarev RV (2002) Observation of coupled magnetic and electric domains. *Nature* 419:818–820. <https://doi.org/10.1038/nature01077>
- Hill NA (2000) Why are there so few magnetic ferroelectrics? *J Phys Chem B* 104:6694–6709. <https://doi.org/10.1021/jp000114x>
- Chakraborty S, Mukherjee S (2015) Studies on dielectric and ferroelectric properties of pure and rare-earth doped nanocrystalline bismuth ferrite. *J Aust Ceram Soc* 51:45–53
- Catalan BG, Scott JF (2009) Physics and applications of bismuth ferrite. *Adv Mater* 21:2463–2485. <https://doi.org/10.1002/adma.200802849>
- Choi T, Lee S, Choi YJ, Kiryukhin V, Cheong SW (2009) Switchable ferroelectric diode and photovoltaic effect in BiFeO_3 . *Science* 324:63–66. <https://doi.org/10.1126/science.1168636>
- Wu H, Zhou J, Liang L, Li L, Zhu X (2014) Fabrication, characterization, properties, and applications of low-dimensional BiFeO_3 nanostructures. *J. Nanomater.* <https://doi.org/10.1155/2014/471485>
- Penalva J, Lazo A (2018) Synthesis of bismuth ferrite BiFeO_3 by solution combustion method. *J Phys Conf Ser.* <https://doi.org/10.1088/1742-6596/1143/1/012025>
- Gao T, Chen Z, Huang Q, Niu F, Huang X, Qin L (2015) A review: preparation of bismuth ferrite nanoparticles and its applications in visible-light induced photocatalyses. *Rev Adv Mater Sci* 40:97–109
- Gao T, Chen Z, Zhu Y, Niu F, Huang Q, Qin L (2014) Synthesis of BiFeO_3 nanoparticles for the visible-light induced photocatalytic property. *Mater Res Bull* 59:6–12. <https://doi.org/10.1016/j.materresbull.2014.06.022>
- Soltani T, Entezari MH (2013) Solar photocatalytic degradation of RB5 by ferrite bismuth nanoparticles synthesized via ultrasound. *Ultrason Sonochem* 20:1245–1253. <https://doi.org/10.1016/j.ultrasonch.2013.01.012>
- Soltani T, Entezari MH (2013) Photolysis and photocatalysis of methylene blue by ferrite bismuth nanoparticles under sunlight irradiation. *J Mol Catal A Chem* 377:197–203. <https://doi.org/10.1016/j.molcata.2013.05.004>
- Wang X, Lin Y, Ding X, Jiang J (2011) Enhanced visible-light-response photocatalytic activity of bismuth ferrite nanoparticles. *J Alloys Compd* 509:6585–6588. <https://doi.org/10.1016/j.jallcom.2011.03.074>
- Hu Y, Fei L, Zhang Y, Yuan J, Wang Y, Gu H (2011) Synthesis of bismuth ferrite nanoparticles via a wet chemical route at low temperature. *J Nanomater.* <https://doi.org/10.1155/2011/797639>
- Ilić NI, Džunuzović AS, Bobić JD, Stojadinović BS, Hammer P, Vijatović Petrović MM (2015) Structure and properties of chemically synthesized BiFeO_3 . Influence of fuel and complexing agent. *Ceram Int* 41:69–77. <https://doi.org/10.1016/j.ceramint.2014.08.020>
- Das N, Majumdar R, Sen A, Maiti HS (2007) Nanosized bismuth ferrite powder prepared through sonochemical and micro-emulsion techniques. *Mater Lett* 61:2100–2104. <https://doi.org/10.1016/j.matlet.2006.08.026>
- Gao F, Chen X, Yin K, Dong S, Ren Z, Yuan F (2007) Visible-light photocatalytic properties of weak magnetic BiFeO_3 nanoparticles. *Adv Mater* 19:2889–2892. <https://doi.org/10.1002/adma.200602377>
- Palchaevev DK, Faradzheva MP, Sadykov SA, Rabadanov MK, Murlieva ZK, Kallaevev SN (2014) Peculiarities of dielectric properties of nanocrystalline bismuth ferrite. *Tech Phys Lett* 40:961–964. <https://doi.org/10.1134/S106378501411008X>
- Patil RP, Delekar SD, Mane DR, Hankare PP (2013) Synthesis, structural and magnetic properties of different metal ion substituted nanocrystalline zinc ferrite. *Results Phys* 3:129–133. <https://doi.org/10.1016/j.rinp.2013.08.002>
- Bhushan B, Basumallick A, Bandopadhyay SK, Vasanthacharya NY, Das D (2009) Effect of alkaline earth metal doping on thermal, optical, magnetic and dielectric properties of BiFeO_3 nanoparticles. *J Phys D Appl Phys* 42:65004. <https://stacks.iop.org/0022-3727/42/i=6/a=065004>. Accessed 3 Mar 2009
- Fu C, Huo M, Cai W, Deng X (2012) Preparation of bismuth ferrite nanopowders at different calcination temperatures. *J Ceram Process Res* 13:561–564
- Shokrollahi H (2013) Magnetic, electrical and structural characterization of BiFeO_3 nanoparticles synthesized by co-precipitation. *Powder Technol* 235:953–958. <https://doi.org/10.1016/j.powtec.2012.12.008>
- Ortiz-Quinonez JL, Díaz D, Zumeta-Dubé I, Arriola-Santamaría H, Betancourt I, Santiago-Jacinto P (2013) Easy synthesis of high-purity BiFeO_3 nanoparticles: new insights derived from the structural, optical, and magnetic characterization. *Inorg Chem* 52:10306–10317. <https://doi.org/10.1021/ic400627c>
- Singh JP, Srivastava RC, Agrawal HM (2010) Optical behaviour of zinc ferrite nanoparticles. *AIP Conf Proc* 1276:137–143. <https://doi.org/10.1063/1.3504278>
- Avinash BS, Chaturmukha VS, Jayanna HS, Naveen CS, Rajeeva MP, Harish BM (2016) Effect of particle size on band gap and DC electrical conductivity of TiO_2 nanomaterial, 020426. <https://doi.org/10.1063/1.4946477>
- Lu J, Qiao LJ, Fu PZ, Wu YC (2011) Phase equilibrium of Bi_2O_3 - Fe_2O_3 pseudo-binary system and growth of BiFeO_3 single crystal. *J Cryst Growth* 318:936–941. <https://doi.org/10.1016/j.jcrysgro.2010.10.181>
- Fu C, Sun F, Hao J, Gao R, Cai W, Chen G (2016) The growth, enhanced optical and magnetic response of BiFeO_3 nanorods synthesized by hydrothermal method. *J Mater Sci Mater Electron* 27:8242–8246. <https://doi.org/10.1007/s10854-016-4830-9>
- Maleki A, Rahimi R, Maleki S (2014) Synthesis, characterization and morphology of new magnetic fluorochromate hybrid nanomaterials with triethylamine surface modified iron oxide nanoparticles. *Synth Met* 194:11–18. <https://doi.org/10.1016/j.synthmet.2014.04.013>

31. Xu Q, Hu C, Wang J, Du J, Xu Q, Hu C (2017) Enhanced ferromagnetism in BiFeO₃ powders by rapid combustion of graphite powders. AIP Adv 055803:1–6. <https://doi.org/10.1063/1.4972806>
32. Biasotto G, Simões A, Foschini C, Antônio S, Zaghete M, Varela J (2011) A novel synthesis of perovskite bismuth ferrite nanoparticles. Process Appl Ceram 5:171–179. <https://doi.org/10.2298/PAC1103171B>
33. Fukumura H, Matsui S, Harima H, Takahashi T, Itoh T, Kisoda K (2007) Observation of phonons in multiferroic BiFeO₃ single crystals by Raman scattering. J Phys Condens Matter 19:365224. <https://doi.org/10.1088/0953-8984/19/36/365224>

Publisher's Note Springer Nature remains neutral with regard to jurisdictional claims in published maps and institutional affiliations.